Research Resource: Small RNA-seq of Human Granulosa Cells Reveals miRNAs in FSHR and Aromatase Genes

Agne Velthut-Meikas, Jaak Simm, Timo Tuuri, Juha S. Tapanainen, Madis Metsis, and Andres Salumets

Competence Center on Reproductive Medicine and Biology (A.V.-M., M.M., A.S.) Tartu 50410, Estonia; Center for Biology of Integrated Systems (A.V.-M., J.S.), Tallinn University of Technology, Tallinn 12618, Estonia; Department of Obstetrics and Gynaecology (A.V.-M., A.S.), University of Tartu, Tartu 51014, Estonia; Department of Obstetrics and Gynecology (T.T., J.S.T.), University of Helsinki and Helsinki University Central Hospital, Helsinki 00029, Finland; Department of Obstetrics and Gynecology and Clinical Research Center (J.S.T.), University of Oulu and Oulu University Hospital, Oulu 90014, Finland; Institute of Mathematics and Natural Sciences (M.M.), Tallinn University, Tallinn 10120, Estonia; and Institute of Biomedicine (A.S.), University of Tartu, Tartu 51014, Estonia

The granulosa cells in the mammalian ovarian follicle respond to gonadotropin signaling and are involved in the processes of folliculogenesis and oocyte maturation. Studies on gene expression and regulation in human granulosa cells are of interest due to their potential for estimating the oocyte viability and in vitro fertilization success. However, the posttranscriptional gene expression studies on micro-RNA (miRNA) level in the human ovary have been scarce. The current study determined the miRNA profile by deep sequencing of the 2 intrafollicular somatic cell types: mural and cumulus granulosa cells (MGCs and CGCs, respectively) isolated from women undergoing controlled ovarian stimulation and in vitro fertilization. Altogether, 936 annotated and 9 novel miRNAs were identified. Ninety of the annotated miRNAs were differentially expressed between MGCs and CGCs. Bioinformatic prediction revealed that TGFβ, ErbB signaling, and heparan sulfate biosynthesis were targeted by miRNAs in both granulosa cell populations, whereas extracellular matrix remodeling, Wnt, and neurotrophin signaling pathways were enriched among miRNA targets in MGCs. Two of the nine novel miRNAs found were of intronic origin: one from the aromatase and the other from the FSH receptor gene. The latter miRNA was predicted to target the activin signaling pathway. In addition to revealing the genome-wide miRNA signature in human granulosa cells, our results suggest that posttranscriptional regulation of gene expression by miRNAs could play an important role in the modification of gonadotropin signaling. miRNA expression studies could therefore lead to new prognostic markers in assisted reproductive technologies. **(*Molecular Endocrinology* 27: 1128–1141, 2013)**

Mammalian ovarian follicles undergo substantial changes including recruitment, extensive expansion, maturation, rupture of follicular membranes during ovulation, development into corpus luteum, and final atresia. These processes are controlled by gonadotropin secretion from the pituitary and intertwining signaling networks between the oocyte and the somatic cells in the ovary.

Inside the follicle 2 somatic cell types can be clearly distinguished: the mural granulose cells (MGCs) and cu-

ISSN Print 0888-8809 ISSN Online 1944-9917
Printed in U.S.A.

Received March 6, 2013. Accepted April 26, 2013.
First Published Online May 9, 2013

Abbreviations: ACVR2B, activin A receptor type IIB; BDNF, brain-derived growth factor; CGC, cumulus granulose cell; Chr, chromosome; COC, cumulus-oocyte complex; ECM, extracellular matrix; FDR, false discovery rate; FSHR, FSH receptor; hCG, human chorionic gonadotropin; HS3ST1, heparin sulfate 3-*O*-sulfotransferase; HSPG, heparan sulfate proteoglycan; KEGG, Kyoto Encyclopedia of Genes and Genomes; ICSI, intracytoplasmic sperm injection; IPA, Ingenuity Pathway Analysis; IVF, in vitro fertilization; MGC, mural granulosa cell; miRNA, micro-RNA; NGS, next-generation sequencing; OPU, ovarian puncture; poly(A) RNA, polyadenylated RNA; pre-miRNA, precursor miRNA.

mulus granulosa cells (CGCs). These cells derive from the same population of early follicles, but differentiate into 2 subpopulations separated by distance by the preovulatory stage (1, 2). CGCs remain close to the oocyte with the inner layer forming adhesive and gap junction transzonal projections that allow trafficking of metabolites between the somatic cells and the oocyte (3, 4). The oocyte secretes several signaling molecules that influence mitogenic processes and the differentiation of CGC (reviewed in Ref. 5). Collectively, oocyte and CGCs form the cumulus-oocyte complex (COC) that remains intact during ovulation up to fertilization (6, 7). MGCs receive weaker signals from the oocyte due to their distance: these cells establish the inner lining of the follicular basal lamina and are responsible for the steroidogenic activity of the maturing follicle (1). In addition, MGCs express receptors for LH necessary for triggering the final maturation of the follicle and ovulatory processes (8).

The intrafollicular cells can be collected without additional inconvenience during oocyte collection procedure from women undergoing in vitro fertilization (IVF) with intracytoplasmic sperm injection (ICSI), and the data obtained from the collected material give valuable information on the regulation of final stages of follicle maturation. By determining the signals that trigger the processes of folliculogenesis during IVF cycles, new ways to improve the efficiency of stimulation as well as new markers for predicting oocyte viability can be found.

The signaling cascades underlying the processes during folliculogenesis have been extensively studied on several model organisms as well as human samples (9–14). However, advances in the knowledge regarding posttranscriptional regulation of mRNAs would make it possible to better predict the actual composition of signaling molecules in the cell. A group of highly conserved posttranscriptional regulators of gene expression are mature micro-RNAs (miRNAs). These are small RNAs, on average 21 nucleotides long, that act by binding to target mRNAs in the RNA-induced silencing complex followed by translational suppression, or mRNA degradation (reviewed in Ref. 15). Preceding the described final outcome, miRNAs undergo several stages of processing. Up to several kilobases long, primary miRNAs are transcribed from the miRNA genes, processed into hairpin-like precursor miRNAs (pre-miRNAs) by DGCR8/Drosha protein complex, and ultimately cut into final length by endoribonuclease Dicer. The last stages of miRNA maturation involve the loading of the short RNA duplex into RNA-induced silencing complex and the degradation of the star strand partially complementary to the mature miRNA sequence (reviewed in Ref. 16). During the last years, alternative pathways of miRNA generation have been revealed, showing that some pre-miRNAs derive from short introns after alternative splicing, and others do not require processing by Dicer (reviewed in Refs. 17 and 18).

The modification of signaling pathways by miRNAs may have considerable importance during ovarian folliculogenesis: abnormal follicle recruitment and maturation were observed in conditional knock-out mice, in which the Dicer1 gene was deleted from all cells expressing the anti-Müllerian hormone receptor (Amhr), including the ovarian granulosa cells (19). In addition, increased follicular atresia, reduced ovulation rates, and compromised oocyte and embryo integrity were observed in these mice by 2 independent investigators (19, 20). Another study reporting an inbred mouse line with hypomorphic Dicer1 evidenced decreased progesterone secretion from corpora lutea leading to infertility (21). However, the ovulation processes were not hampered in this model.

High-throughput miRNA profile analysis from different ovarian somatic cell types appears rare among the publications so far. To our knowledge, one sequencing study on human postmortem ovarian homogenate has been published (22). There is slightly more data from model organisms comparing the miRNA profiles between the bovine ovarian and testis tissues (23) and different stages of the corpus luteum (24), ovine follicle homogenates from various stages of folliculogenesis (25), porcine atretic and normal follicles (26), and cultured rat granulosa cells upon FSH stimulation (27).

The aim of the current study was to fill the gap in information regarding the miRNA profile in human follicular granulosa cells from IVF patients. We performed our study using next-generation sequencing (NGS) that enabled us to determine annotated as well as novel, yet unannotated, miRNAs. Our goal was to examine the degree of difference between MGCs and CGCs regarding their miRNA profile and to predict the potential targets of annotated and novel miRNAs in either cell type. In addition, the polyadenylated RNA (poly[A] RNA) population from the same samples was sequenced in order to acquire further biological confirmation for the predicted miRNA targets.

Materials and Methods

Patients and stimulation protocol

The study was approved by the Ethics Committee of the University of Tartu in Estonia, and informed consent was obtained from all participants. Three women, aged 31.3 ± 3.1 years (mean ± SD), undergoing ICSI and embryo transfer at Nova Vita Clinic (Tallinn, Estonia) were enrolled. Due to male factor infertility, all patients had been unable to conceive for at least 1 year before entering the study.

Ovarian hormonal stimulation was conducted according to the GnRH antagonist (Cetrotide; Merck Serono, Geneva, Switzerland) protocol with the administration of recombinant FSH (Gonal-F; Merck Serono or Puregon, Schering-Plough, Kenilworth, New Jersey). On average, 1316.7 ± 401.0 IU of FSH was used during the 9.0 ± 1.0 days of ovarian stimulation. All patients underwent ovarian puncture (OPU) of follicles ≥15 mm in size after 36 hours of human chorionic gonadotropin (hCG) administration (Ovitrelle, Merck Serono). The total number of oocytes retrieved from each patient was 17.3 ± 7.1, of which 17.0 ± 7.5 were considered mature at metaphase II stage (97.0 ± 5.2% of all). ICSI was used to fertilize the oocytes 4–6 hours after OPU with 73.4% of oocytes fertilized. Up to 2 (1.7 ± 0.6) second (n = 2) or third (n = 1) day embryos were transferred, resulting in one patient achieving a clinical pregnancy.

The control group used for confirming the differential and novel miRNA expression consisted of samples from 8 additional IVF patients with the following characteristics: age 31.0 ± 6.2 years, FSH amount used was 1528.0 ± 653.8 IU, the number of retrieved oocytes was 12.0 ± 9.1, of which 75.0 ± 22.2% were mature and 66.7 ± 10.9% fertilized normally. All women underwent IVF-ICSI due to male factor infertility, and 2 of them had been additionally diagnosed with tubal infertility.

Granulosa cell isolation

MGCs were obtained from follicular fluid after OPU following the manual removal of COC and CGC aggregates devoid of the oocyte. The fluid from all follicles of a patient was pooled, centrifuged at 450 × *g* for 10 minutes, followed by supernatant removal. The cells were separated on a 50% density gradient of PureSperm 100 (Nidacon; Mölndal, Sweden) in Universal IVF Medium (Origio; Jyllinge, Denmark), washed 3 times in Universal IVF Medium at 37°C, depleted of CD45-positive leukocytes according to the manufacturer's suggested protocol (DynaMag and Dynabeads; Life Technologies, Carlsbad, California), lysed with QIAGEN miRNeasy Mini kit lysis buffer (QIAGEN, Hilden, Germany), and stored in liquid nitrogen for future use.

CGCs were collected and processed as described in detail in our previous publication (13).

RNA extraction and quality control (QC)

Total RNA and small RNA from MGCs and CGCs were extracted using the miRNeasy Mini Kit (QIAGEN), according to the manufacturer's instructions. The quantity and purity of each RNA sample were assessed with spectrophotometer NanoDrop ND-10 (Thermo Fisher Scientific, Wilmington, Delaware). RNA integrity was analyzed using the RNA 6000 Nano Kit and Small RNA Kit with the 2100 Bioanalyzer (Agilent Technologies, Palo Alto, California). All samples were of high quality with the absorbance wavelength ratio (A260/A280) of ≥1.9 and the RNA Integrity Number of ≥8.6. On average, 1 μg of RNA was used as starting material for poly(A) RNA library preparation, and 100 ng for small RNA library preparation.

Library preparation and sequencing

Library preparation and sequencing was performed at Biomedicum Functional Genomics Unit at the University of Helsinki in Finland. The detailed protocol is described in Supplemental Materials and Methods published on The Endocrine Society's Journals Online web site at http://mend.endojournals.org. In brief, separate libraries were prepared for small RNA and poly(A) RNA population from the same samples. Unique adapters from NEXTflex DNA Barcodes (Bioo Scientific Corp, Austin, Texas) were ligated to separate samples for further indexing, after which all 6 samples were pooled. After PCR amplification and cluster generation, paired-end sequencing of 101 bp read length was performed with HiSeq 2000 (Illumina, Inc, San Diego, California) for poly(A) RNA libraries, and 36-bp single reads were acquired on Genome Analyzer IIx (Illumina) from small RNA libraries. Small RNA libraries were sequenced twice, and the acquired data are further considered as technical replicates.

Sequencing data analysis of poly(A) RNA samples

The pipeline for sequencing data analysis is described in detail in Supplemental Materials and Methods. The number of raw reads for each gene acquired via the described pipeline was used as input for R/Bioconductor package EdgeR (28, 29) for performing differential expression analysis between MGC and CGC samples. Genes with less than 0.1 counts per million in all samples were discarded, and false discovery rate (FDR) less than 5% was considered as statistically significant after multiple testing correction.

Sequencing data analysis of small RNA samples

Raw filtered data was submitted to miRDeep2 software (30) that integrates adapter trimming, sequence alignment, and miRNA annotation according to miRBase version 18. Further, novel miRNAs are predicted by miRDeep2 upon the detection of potential mature, star and loop sequences from the read pool, and hairpin formation stability of the potential miRNA precursor according to the RNAfold algorithm (31). Default parameters were used in all steps. Similarity search between potential novel miRNAs and human mature miRNA sequences in the miRBase database was performed by BLASTN algorithm online (www.mirbase.org). Significant multiple alignments were visualized in Jalview v.2.8 software (32).

Differential miRNA expression analysis was performed by EdgeR as described for poly(A) RNA data analysis, except that the reads for technical replicates were summed, and miRNAs with less than 10 raw counts in all samples were discarded.

All data obtained via NGS is available at Gene Expression Omnibus data repository, accession number GSE46508 (http://www.ncbi.nlm.nih.gov/geo/).

Validation of miRNA expression by real-time RT-PCR

A selection of miRNAs showing statistically significant expression level differences between MGCs and CGCs in sequencing data was validated by predesigned real-time RT-PCR assays (Exiqon, Vedbaek, Denmark). cDNA was synthesized from 20 ng of small RNA from 8 patients from the control group using the Universal cDNA Synthesis Kit, and real-time RT-PCR was performed in triplicates with Universal RT SYBR Green Mastermix according to the manufacturer's protocols (Exiqon). 7900 HT real-time PCR System and SDS 2.3 software were used to run the reactions (Applied Biosystems, Foster City, California). Eight annotated miRNAs were tested: hsa-miR-30a-5p, hsa-miR-142-5p, hsa-miR-126-3p, hsa-miR-223-3p, hsa-miR-

874, hsa-miR196a-5p, hsa-miR129-5p, hsa-miR-129-3p, normalized for hsa-miR-132–3p and analyzed for expression differences between MGCs and CGCs according to the ΔΔCt method.

Validation of 4 novel miRNAs was performed on the above-described conditions with custom made real-time PCR assays (Exiqon). In addition, synthetic RNA oligonucleotides with 5′-end phosphate group corresponding to the mature sequences of the tested miRNAs were used as positive controls (Integrated DNA Technologies, Inc, Coralville, Iowa).

Bioinformatic prediction of miRNA targets

Two approaches were used for predicting annotated miRNA target genes and pathways. First, the lists of differentially expressed miRNAs were uploaded into DIANA miRPath version 2.1 (33), a web-based software that is updated to miRBase v18 and uses the microT-CDS algorithm for calculating miRNA binding sites in the 3′-untranslated region as well as the coding region of the mRNAs. It further predicts enriched signaling pathways of the submitted miRNA targets using the Kyoto Encyclopedia of Genes and Genomes (KEGG) database (34). Because the list of MGC miRNAs was longer than that of CGC miRNAs, only the top 33 miRNAs were used in order not to analyze significantly more targets from MGCs. Conservative parameters were chosen for acquiring the union list of predicted target genes (a priori method): MicroT score threshold was set to 0.9, *P* value was set to .05, and both the Benjamini and Hochberg FDR and the conservative statistics options were used. Subsequently, the acquired KEGG pathways were studied for their enrichment of genes that were differentially expressed at mRNA level from our poly(A) RNA NGS experiment. Pathways with less than 10% of genes providing proof from the experiment were discarded because they were considered to turn up in the analysis by chance.

The second approach was used to analyze data from our sequencing experiments only. Analysis was performed by Ingenuity Pathway Analysis (IPA) Software (Ingenuity Systems, Inc., Redwood City, California) and is described in detail in Supplemental Materials and Methods.

In order to predict targets for novel miRNAs, DIANA microT v3.0 (35, 36) that accepts novel potential miRNA mature sequences as input was used. All predicted targets with a score greater than 7.35 for each novel miRNA were further submitted to The Database for Annotation, Visualization and Integrated Discovery (DAVID) v6.7 (37, 38), where the list was further enriched for gene ontology terms according to biologic process, cellular compartment, or molecular function. FDR less than 5% was used as a cut-off for statistical significance in DAVID in all cases.

Results

NGS outcome parameters and the description of the most abundant miRNAs

In addition to studying the miRNA profile of ovarian somatic cells, we also attempted to predict their potential targets and confirm these using experimental data. For that reason, small RNA and poly(A) RNA sequencing was performed from the same samples, and technical data from the experiments are summarized in Supplemental Table 1.

Table 1. Top 10 Lists of Most Abundant miRNAs in MGCs (A) and CGCs (B)

A		B	
miRNA	Average rpm in MGCs	miRNA	Average rpm in CGCs
hsa-miR-21-5p	69080.68	*hsa-miR-21-5p*	89927.85
hsa-let-7f-5p	40089.97	*hsa-miR-99a-5p*	28689.39
hsa-miR-451a	16549.71	*hsa-let-7f-5p*	14219.34
hsa-miR-30a-5p	15931.49	*hsa-miR-26a-5p*	10606.24
hsa-miR-99a-5p	15257.67	hsa-let-7a-5p	8057.85
hsa-let-7g-5p	14633.43	*hsa-miR-451a*	7119.30
hsa-miR-26a-5p	12858.71	*hsa-miR-191-5p*	6382.17
hsa-miR-27b-3p	8324.83	hsa-miR-22-3p	5731.12
hsa-miR-486-5p	7730.59	hsa-miR-146b-5p	5424.98
hsa-miR-191–5p	6858.22	*hsa-let-7g-5p*	5324.91

Expression is presented as average reads per million reads (rpm). Common miRNAs in two lists are printed in italic.

Altogether, we identified 1039 annotated mature miRNAs with at least 1 raw read in at least 1 sample: 936 in MGCs and 883 in CGCs (Supplemental Table 2). The most abundant miRNAs in either cell population are presented in Table 1. Seven miRNAs are common between these lists, and the remaining 3 can be found among the top 22 most abundant miRNAs of the other cell type (Supplemental Table 2). Hsa-miR-21-5p was clearly the most abundant miRNA in both MGCs and CGCs. From poly(A) sequencing data we identified mRNAs corresponding to 22 629 genes in MGCs and 22 554 genes in CGCs. Among those, we found evidence of hairpin sequences for several miRNAs detected from the small RNA library (Supplemental Table 2). The full list of transcripts is available at Gene Expression Omnibus data repository.

Based on both miRNA and mRNA expression profiles, the samples clustered together on a multidimensional scaling plot according to the individual patients and the cell type from which the RNA was extracted (Supplemental Figure 1, A and C). This result was also confirmed upon hierarchical clustering on heat maps (Supplemental Figure 1, B and D).

Differentially expressed annotated miRNAs and their targeted pathways

Ninety miRNAs were differentially expressed with statistical significance: 33 revealed higher expression levels in CGCs and 57 in MGCs (Table 2). The expression levels of 8 miRNAs were also validated by real-time RT-PCR and normalized for hsa-miR-132-3p for which the smallest relative standard deviation was calculated from NGS

Table 2A. Differentially Expressed miRNAs According to FDR < 0.05. A: List of miRNAs Up-regulated in MGC.

No.	miRNA	FC (MGC/CGC)	FDR
1	hsa-miR-548ap-5p	5.97	0.0068
2	hsa-miR-548j	5.97	0.0068
3	hsa-miR-539-3p	3.71	0.0007
4	hsa-miR-142-5p	3.56	0.0002
5	hsa-miR-144-5p	3.37	0.0024
6	hsa-miR-126-5p	3.30	0.0060
7	hsa-miR-126-3p	3.17	0.0007
8	hsa-miR-487a	3.05	0.0114
9	hsa-miR-454-5p	2.95	0.0068
10	hsa-miR-223-3p	2.87	0.0009
11	hsa-miR-624-5p	2.87	0.0047
12	hsa-miR-30a-5p	2.83	0.0029
13	hsa-miR-335-5p	2.80	0.0068
14	hsa-miR-889	2.77	0.0041
15	hsa-miR-10b-3p	2.76	0.0374
16	hsa-miR-154-5p	2.72	0.0210
17	hsa-miR-655	2.69	0.0271
18	hsa-miR-4732-5p	2.68	0.0308
19	hsa-miR-32-5p	2.64	0.0167
20	hsa-miR-451a	2.62	0.0136
21	hsa-let-7i-3p	2.59	0.0392
22	hsa-miR-10b-5p	2.57	0.0068
23	hsa-miR-20b-5p	2.56	0.0068
24	hsa-miR-30a-3p	2.55	0.0068
25	hsa-miR-196b-5p	2.54	0.0271
26	hsa-miR-363-3p	2.52	0.0103
27	hsa-miR-429	2.49	0.0302
28	hsa-miR-194-5p	2.46	0.0121
29	hsa-miR-223-5p	2.43	0.0400
30	hsa-miR-379-5p	2.42	0.0128
31	hsa-miR-584-5p	2.41	0.0128
32	hsa-miR-656	2.40	0.0374
33	hsa-miR-106a-5p	2.38	0.0075
34	hsa-miR-144-3p	2.38	0.0271
35	hsa-miR-146a-5p	2.36	0.0128
36	hsa-miR-487b	2.35	0.0149
37	hsa-miR-142-3p	2.34	0.0308
38	hsa-miR-324-5p	2.34	0.0374
39	hsa-miR-377-3p	2.32	0.0257
40	hsa-miR-369-3p	2.31	0.0271
41	hsa-miR-374a-5p	2.28	0.0257
42	hsa-miR-409-5p	2.25	0.0084
43	hsa-miR-548b-5p	2.24	0.0308
44	hsa-miR-1185-2-3p	2.23	0.0480
45	hsa-miR-29b-3p	2.20	0.0257
46	hsa-miR-382-3p	2.20	0.0402
47	hsa-miR-494	2.19	0.0125
48	hsa-miR-98	2.19	0.0233
49	hsa-miR-199b-5p	2.17	0.0257
50	hsa-miR-10a-5p	2.14	0.0271
51	hsa-miR-335-3p	2.11	0.0404
52	hsa-miR-411-5p	2.07	0.0271
53	hsa-let-7f-2-3p	2.02	0.0385
54	hsa-miR-96-5p	1.96	0.0271
55	hsa-miR-483-3p	1.94	0.0302
56	hsa-miR-340-5p	1.93	0.0437
57	hsa-miR-16-5p	1.87	0.0302

(*Continued*)

Table 2B: List of miRNAs Up-regulated in CGCs

No.	miRNA	FC (MGC/CGC)	FDR
1	hsa-miR-129-2-3p	−6.58	0.0000
2	hsa-miR-129-5p	−5.57	0.0000
3	hsa-miR-1273e	−3.86	0.0010
4	hsa-miR-4488	−3.62	0.0082
5	hsa-miR-4461	−3.61	0.0068
6	hsa-miR-181a-2-3p	−3.60	0.0001
7	hsa-miR-1290	−3.46	0.0010
8	hsa-miR-34c-3p	−3.41	0.0121
9	hsa-miR-196a-5p	−3.31	0.0009
10	hsa-miR-4792	−3.17	0.0091
11	hsa-miR-874	−3.11	0.0006
12	hsa-miR-3651	−3.07	0.0009
13	hsa-miR-135a-5p	−3.05	0.0098
14	hsa-miR-873-3p	−3.04	0.0047
15	hsa-miR-1291	−2.93	0.0011
16	hsa-miR-876-5p	−2.70	0.0154
17	hsa-miR-181a-3p	−2.66	0.0065
18	hsa-miR-1275	−2.62	0.0241
19	hsa-miR-4497	−2.43	0.0352
20	hsa-miR-181c-3p	−2.29	0.0257
21	hsa-miR-320c	−2.25	0.0245
22	hsa-miR-23b-5p	−2.24	0.0302
23	hsa-miR-378g	−2.18	0.0462
24	hsa-let-7c	−2.14	0.0271
25	hsa-miR-320d	−2.12	0.0344
26	hsa-miR-1292	−2.08	0.0480
27	hsa-miR-125b-5p	−2.04	0.0245
28	hsa-miR-181b-5p	−2.01	0.0302
29	hsa-miR-320b	−1.99	0.0271
30	hsa-miR-202-3p	−1.92	0.0257
31	hsa-miR-1180	−1.91	0.0346
32	hsa-miR-4485	−1.87	0.0305
33	hsa-miR-181a-5p	−1.73	0.0374

FC, fold change in $\log_2$ scale.

results. Samples from 8 women distinct from the NGS experiment were used. According to real-time PCR experiment, 6 miRNAs were differentially expressed with statistical significance, whereas the remaining 2 showed the same trend as in NGS experiment (Supplemental Figure 2A). Differential expression of poly(A) RNAs was compared with the results of our previous study on the Affymetrix GeneChip Human Gene 1.0 ST Array (13). A high positive correlation value of 0.82 was achieved when comparing the 2 datasets with a P value $<2.2 \times 10^{-16}$ (Supplemental Figure 3).

Besides observing a number of miRNAs that were differentially expressed between MGC and CGC, we were interested in the signaling pathways and biological functions that could potentially be targeted by them. Because there are tens of algorithms available for the bioinformatic prediction of miRNA targets, we decided for two different approaches. Firstly, we used DIANA miRPath that is updated to miRBase v.18, the same version that was used for annotating known miRNAs from our NGS data. We allowed the software to predict miRNA target

genes, performed the enrichment of KEGG pathways from the predicted targets and then compared the results with our poly(A) RNA data (Table 3). This approach allows to observe additional targets that may have been missed by poly(A) RNA NGS due to small sample size and the lack of time-scale data.

Interestingly, there are several common signaling pathways that are targeted by the differentially expressed miRNAs: those involved in TGF-β and ErbB signaling as well as heparan sulfate biosynthesis. From our poly(A) RNA data we find evidence that in MGCs, already the first essential steps of heparan sulfate biosynthesis may be inhibited. More specifically, xylosyltransferase I that transfers the first saccharide unit to the target peptide and exostosin 1 responsible for further polysaccharide chain elongation were down-regulated in MGC on mRNA

Table 3. KEGG Pathways Enriched for Targets of miRNAs That Were Differentially Expressed in MGC (A) and CGC (B) According to DIANA miRPath v.2.1

A

KEGG Pathway	FDR-Adjusted *P* Value	No. of Targeted Genes	No. of miRNAs Targeting the Pathways	Genes Confirmed by Poly(A) RNA NGS
ECM-receptor interaction	1.14E-16	29	22	ITGB8, ITGB3, ITGA5, THBS1, COL5A1, COL1A2, FN1
TGF-β signaling pathway	1.35E-09	37	24	THBS1, PITX2, ACVR1, ACVR2B, E2F5, LTBP1, SMAD7
Endocytosis	5.22E-09	72	26	CBL, CAV1, NEDD4L, RAB31, PSD3, FLT1, NEDD4, DNM3, SMAD7, ADRB1, ASAP2
Glycosaminoglycan biosynthesis - heparan sulfate	1.11E-06	10	9	EXT1, XYLT1
Focal adhesion	0.0005	65	27	ITGB8, THBS1, CAV1, ITGB3, ITGA5, MAPK8, COL5A1, FLT1, COL1A2, FN1
Neurotrophin signaling pathway	0.0025	46	26	SORT1, BDNF, YWHAQ, RPS6KA5, MAPK8, CAMK2B
Wnt signaling pathway	0.0035	46	26	FZD7, WNT16, APC, FZD3, MAPK8, CAMK2B, WIF1, DAAM1
Axon guidance	0.0065	40	25	PLXNA2, EPHA5, CXCL12, SEMA6B, EPHA3, NCK2, SEMA3A, NTN4, GNAI1, EFNA1
ErbB signaling pathway	0.0070	30	25	CBL, NCK2, MAPK8, CAMK2B
Endocrine and other factor-regulated calcium reabsorption	0.0251	15	16	KL, DNM3
N-Glycan biosynthesis	0.0290	13	13	ST6GAL2, MGAT3
Amoebiasis	0.0308	28	20	ARG2, COL5A1, COL1A2, FN1
Mucin type *O*-glycan biosynthesis	0.0342	7	9	GALNT3

B

KEGG Pathway	FDR-Adjusted *P* Value	No. of Targeted Genes	No. of miRNAs Targeting the Pathways	Genes Confirmed by Poly(A) RNA NGS
Glycosaminoglycan biosynthesis - heparan sulfate	2.60E-07	6	6	HS3ST1
Lysine degradation	4.80E-06	14	13	TMLHE, SUV39H1
TGF-β signaling pathway	0.0006	27	14	ID4, DCN, BMP8A, TGFBR2
ErbB signaling pathway	0.0395	26	18	TGFA, PAK7, SHC4, ERBB4, EREG
Glioma	0.0423	17	13	TGFA, IGF1, SHC4,

Italic text represents common pathways between MGC and CGC. NGS, next-generation sequencing.

Table 4. Novel miRNAs Predicted from Small RNA Sequencing Data by miRDeep2

miRNA Identification	Mature Sequence	Average Read Count in MGCs	No. of Samples Detected in MGCs	Average Read Count in CGCs	No. of Samples Detected in CGCs	Predicted Hairpin Genomic Coordinates and Strand	Predicted Hairpin Genomic Region
Chr1.1	uuucaggucuggggcugaaaccu	18.3	3	48.7	3	chr1:113424681..113424744:+	Intergenic
Chr2.1[#]	aaagguaacugugauuuuugcu	46.3	3	114	3	chr2:49286742..49286798:+	FSHR gene intron
Chr15.1a[##]	ugugacccuagaauaauuac	34.3	3	11	1	chr15:51606231..51606307:+	CYP19A1 gene intron
Chr15.1b[###]	ugugacccuagaauaauuac	34.3	3	11	1	chr15:51606228..51606304:−	CYP19A1 gene intron
Chr19.1[$]	aggcugugaugcucuccugagccc	43	3	217.7	3	chr19:11606358..11606437:−	Intergenic
Chr1.2	aguugggagagcauuagacuga	0	0	3.5	2	chr1:213020182..213020250:+	Intergenic
Chr19.2[$$]	auccuagucacggcacca	19	1	3	1	chr19:55634592..55634660:−	Intergenic
Chr3.1*	ugcccugagacuuuugcuc	12.7	3	4	1	chr3:127305953..127306019:−	Intergenic
Chr3.2**	uucccagccaacgcacca	2	1	0	0	chr3:176232891..176232940:+	Intergenic
Chr4.1***	ucugguguauagcguugcuca	0	0	4	1	chr4:21466322..21466381:−	KCNIP4 gene, intronic region

Two versions of Chr1.1 (miRNA on chromosome 1.1) mature sequences were observed with similar prevalence, the difference in 5′-end is underlined. Chr15.1a and Chr15.1b share the same mature sequence. miRNAs in bold were studied in detail (see text).

[#], hsa-miR-548ba.

[##], hsa-miR-7973-1.

[###], hsa-miR-7973-2.

[$], hsa-miR-7974.

[$$], hsa-miR-7975.

*, hsa-miR-7976.

**, hsa-miR-7977.

***, hsa-miR-7978.

level. At the same time, 3-*O*-sulfotransferase (HS3ST1), which performs one of the many possible modifications at a later stage of heparan sulfate biosynthesis, was downregulated in CGC via predicted miRNA targeting.

Although the number of miRNAs uploaded to the software was equal, the number of targets and target pathways was considerably greater for MGCs than for CGCs. Extracellular matrix (ECM) proteins, endocytosis pathways as well as signaling via neurotrophins and Wnt pathways were specifically targeted by miRNAs from MGCs.

As a second approach, we only used data from our own poly(A) RNA NGS experiment to perform the enrichment of miRNA targets. The IPA software merges several target prediction algorithms into 1 environment. The differentially expressed genes from poly(A) RNA NGS results that were considered as highly predicted or experimentally validated targets for differentially expressed miRNAs in our data were further analyzed for their enrichment according to their molecular functions in gene ontology database and signaling pathways from KEGG and Reactome (Supplemental Table 3A).

For MGCs, the results acquired by the described method confirm well the outcome from miRPath. ECM-receptor interaction and axon guidance referring to neurotrophin signaling were also enriched by this approach. In addition, targets were grouped significantly into molecular functions involved in cytoskeletal protein binding, ion binding, and protein kinase activity (Supplemental Table 3A).

In contrast, in CGCs the molecular functions enriched were rather involved in phosphatase activity and transcription factor activity, including steroid hormone receptor activity. For example, estrogen receptor-α (ESR1) is a potential predicted miRNA target in CGCs. Enrichment of signaling pathways was not as successful for CGC as it was for MGC data. Only amino acid metabolism is predicted to be specifically targeted by miRNAs in CGCs according to Reactome (Supplemental Table 3B).

Prediction of novel miRNAs and their targeted pathways

A great advantage of the NGS technology is the possibility of identifying novel transcripts. Therefore, our next aim was to predict novel, unannotated miRNAs from the small RNA data by miRDeep2 software. miRDeep2 predicts the probability of a sequence being a novel miRNA according to its surrounding genomic context and its potential to fold into hairpin-like structure with low free energy characteristic of miRNAs. Although there were several unannotated short sequences in our data, we introduce nine different potential novel miRNAs that were present in both technical replicates of at least 1 sample with a minimal average read count of 2 (Table 4). None of the novel miRNAs aligned with any other classes of small RNA, rRNA, or coding sequences. We further concentrated on 4 potential novel miRNAs with the highest expression values and the most frequent appearance among samples. Those miRNAs aligned on different chromosomes: 1, 2, 15, and 19 and, for the sake of clarity, are further referred to according to the chromosome (Chr)

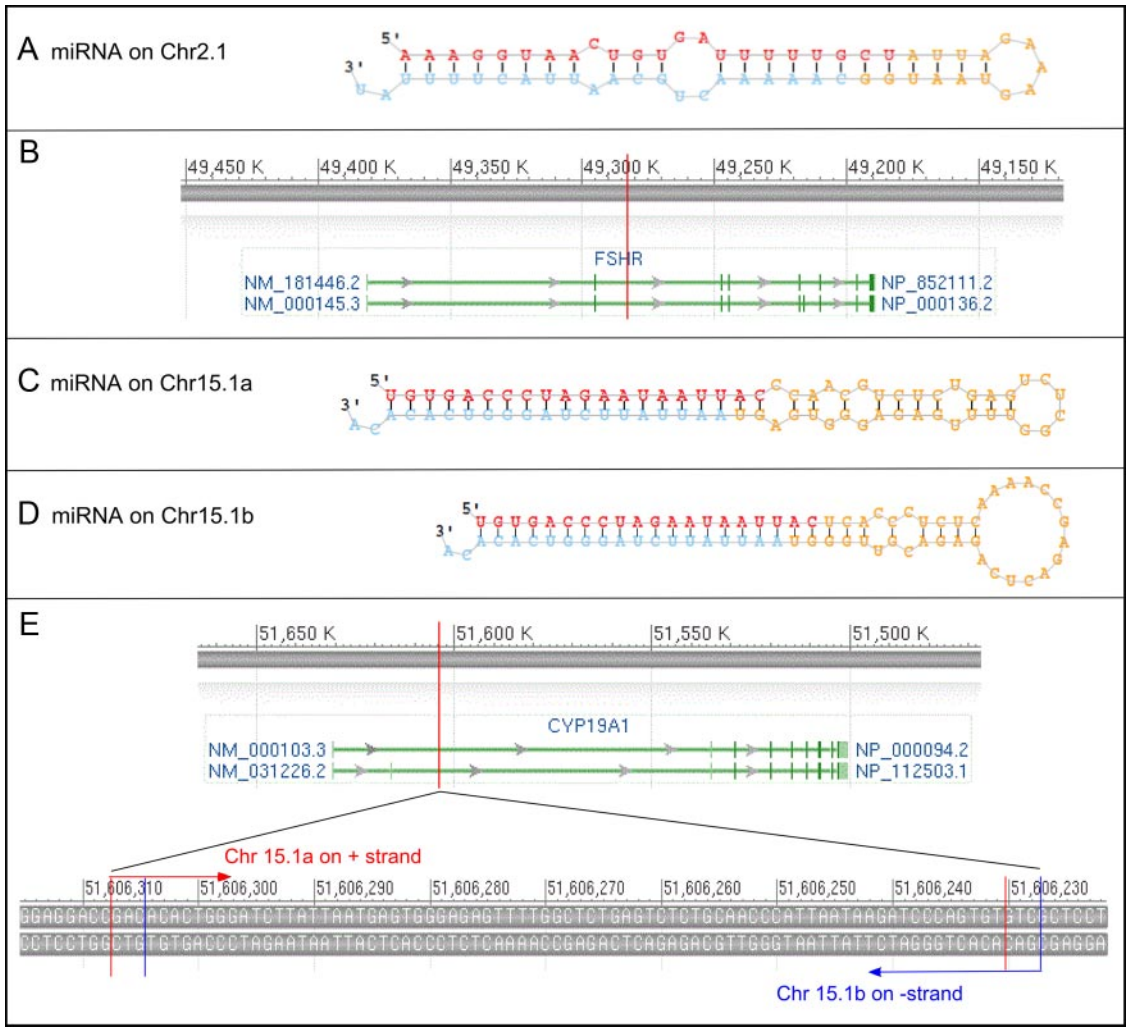

Figure 1. Hairpin Structures and Graphical Representations of pre-miRNA Genomic Locations for Novel miRNAs on Chr2.1, Chr15.1a and 15.1b. A, Hairpin structure of miRNA on Chr2.1. B: Graphical representation of FSHR gene. The transcription site for miRNA on Chr2.1 in the intronic region is marked in red. C and D: Two possible hairpin structures for miRNA on Chr15.1 noted as Chr15.1a and 15.1b. E: Two possible genomic locations for miRNA on Chr15.1 in the intronic region of CYP19A1 gene. Genomic location of miRNA on Chr15.1a is marked in red and Chr15.1b in blue in the subset.

number. We validated the expression of those 4 novel miRNAs by real-time RT-PCR. These miRNAs are expressed in both MGCs and CGCs, and only miRNA on Chr19 was more abundant in CGCs with statistical significance (Supplemental Figure 2B).

miRNAs on Chr1.1 and Chr19.1 are both transcribed from intergenic regions. For miRNA on Chr1.1, two alternative mature reads were observed with similar frequency: a 23-nucleotide read with 3 uridine residues in the 5′-end or a 22-nucleotide read with 2 uridine residues (Table 4). The hairpin of Chr2.1 pre-miRNA structure is depicted in Figure 1A, and its sequence aligned to the intronic region of the FSH receptor (FSHR) gene (Figure 1B). miRNA on Chr15.1 is predicted to be transcribed from an intron of the aromatase gene (CYP19A1). Interestingly, there are 2 possible genomic locations for this miRNA in the same intron, one from the plus (miRNA on Chr15.1a) and the other from the minus strand (miRNA on Chr15.1b), giving rise to 2 slightly different possible hairpins with the same mature sequences (Figure 1, C–E).

We searched for high-similarity sequences for the predicted novel miRNAs in the miRBase online search tool. High similarity with several members of the hsa-miR-548 family was found for the sequence of miRNA on Chr2.1. The highest BLASTN score of 78 was acquired by pairwise alignment between miRNA on Chr2.1 and hsa-miR-548d-5p, hsa-miR-548w, and hsa-miR-548ag as well as hsa-miR548ay-5p. In all of the cases, 3 mismatches appeared in the alignment, and discrepancies in the 3′-ends of the sequences were observed (Figure 2). No other predicted novel miRNAs showed similarities to any annotated human mature miRNAs.

Subsequently we analyzed the potential targets of the

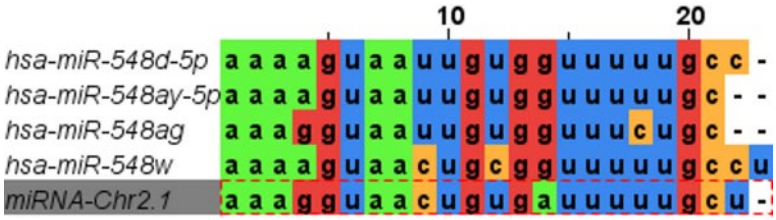

Figure 2. Sequence Alignment between miRNA on Chr2.1 (shaded) and Four Members of the hsa-miR-548 Family. BLASTN score for each pair-wise alignment with Chr2.1 was 78 and e-value was 0.2.

novel miRNAs using DIANA microT v3.0, a web-based software that accepts unannotated user-defined miRNA sequences as input. The potential targets predicted for the 4 miRNAs are available as supplemental material (Supplemental Table 4). Fifty-five targets were predicted for miRNA on Chr1.1, 132 for miRNA on Chr2.1, 20 for miRNA on Chr15.1, and 91 for miRNA on Chr19.1. The enrichment of targets according to gene ontology (biologic processes, molecular functions, and cellular compartments) is presented in Table 5. The targets of miRNA on Chr1.1 are predicted to be cytoskeleton proteins associated with cell morphogenesis. Targets of miRNA on Chr2.1 are involved in response to carbohydrate stimulus, peptide secretion, and gene silencing. One of the predicted targets of this miRNA is DICER mRNA that is further translated into a central protein in miRNA biogenesis. Interestingly, activin A receptor type IIB (ACVR2B) and SMAD2, a component of activin-signaling cascade, are common genes in most of the en-

Table 5. Gene Ontology Terms Enriched by Predicted Novel miRNA Targets

miRNA Identification	Category	Term	Count	Genes	FDR %
Chr1.1	Cellular component	Cytoskeleton	14	LOC651610, DLGAP1, KAZ, TOPBP1, AKAP9, PCM1, TTN, ATM, RAB3IP, PPP1R9A, PAK2, MACF1, MYOM1, EDA, DLG2	0.09
		Cytoskeletal part	10	LOC651610, DLGAP1, PPP1R9A, AKAP9, TOPBP1, MYOM1, TTN, PCM1, DLG2, ATM, RAB3IP	1.49
	Biological process	Cell projection morphogenesis	6	MACF1, ONECUT2, NTNG1, VAX1, PCM1, RAB3IP	1.09
		Cell part morphogenesis	6	MACF1, ONECUT2, NTNG1, VAX1, PCM1, RAB3IP	1.32
		Cellular component morphogenesis	7	MACF1, ONECUT2, NTNG1, VAX1, TTN, PCM1, RAB3IP	1.50
		Cilium assembly	3	ONECUT2, PCM1, RAB3IP	4.47
Chr2.1	Biologic process	Pancreas development	5	ACVR2B, ONECUT2, NEUROD1, SMAD2, PROX1	0.17
		Postembryonic development	6	ACVR2B, MORC3, BCL11B, SMAD2, MECOM, BCL2L11	0.28
		Response to glucose stimulus	5	ACVR2B, NEUROD1, SMAD2, FKBP1B, PTEN, PTENP1	0.47
		Response to hexose stimulus	5	ACVR2B, NEUROD1, SMAD2, FKBP1B, PTEN, PTENP1	0.55
		Response to monosaccharide stimulus	5	ACVR2B, NEUROD1, SMAD2, FKBP1B, PTEN, PTENP1	0.55
		Posttranscriptional regulation of gene expression	8	CPEB2, MORC3, IMPACT, DICER1, QKI, SMAD2, LIN28B, PTEN, PTENP1	1.26
		Response to carbohydrate stimulus	5	ACVR2B, NEUROD1, SMAD2, FKBP1B, PTEN, PTENP1	1.40
		Insulin secretion	4	ACVR2B, NEUROD1, SMAD2, FKBP1B	1.45
		Protein amino acid phosphorylation	14	CDK19, ITK, WNK1, BMPR2, MOBKL1A, ABI2, SMAD2, CDK6, PRKG1, ACVR2B, PAK2, MORC3, COL4A3BP, LOC100132369, EIF2AK2	1.45
		Peptide hormone secretion	4	ACVR2B, NEUROD1, SMAD2, FKBP1B	4.21
		Peptide secretion	4	ACVR2B, NEUROD1, SMAD2, FKBP1B	4.84
		Gene silencing by miRNA, production of miRNAs	3	DICER1, SMAD2, LIN28B	4.96
Chr15.1	None				
Chr19.1	Biologic process	Cellular component morphogenesis	9	RAB8A, TNR, PCNT, NFASC, CNTN2, PIP5K1C, TTN, GAS7, CDH23	0.51
		Cell projection morphogenesis	7	RAB8A, TNR, PCNT, NFASC, CNTN2, PIP5K1C, GAS7	1.09
		Cell part morphogenesis	7	RAB8A, TNR, PCNT, NFASC, CNTN2, PIP5K1C, GAS7	1.37
		Cell morphogenesis	8	RAB8A, TNR, PCNT, NFASC, CNTN2, PIP5K1C, GAS7, CDH23	1.42
		Positive regulation of transcription, DNA-dependent	9	CIITA, PPARA, FOXK1, ZMIZ2, MAML1, PAX8, TEAD1, FOXO1, NR5A2	1.70
		Cell projection organization	8	RAB8A, TNR, PCNT, NFASC, CNTN2, PIP5K1C, GAS7, CDH23	1.72
		Positive regulation of RNA metabolic process	9	CIITA, PPARA, FOXK1, ZMIZ2, MAML1, PAX8, TEAD1, FOXO1, NR5A2	1.80
		Positive regulation of transcription from RNA Pol II promoter	8	CIITA, PPARA, ZMIZ2, MAML1, PAX8, TEAD1, FOXO1, NR5A2	1.80
		Regulation of transcription from RNA Pol II promoter	11	CIITA, PPARA, FOXK1, ZMIZ2, MAML1, PAX8, TEAD1, FOXO1, MDM4, NR5A2, KCNIP3	1.83
		Positive regulation of transcription	9	CIITA, PPARA, FOXK1, ZMIZ2, MAML1, PAX8, TEAD1, FOXO1, NR5A2	4.79
	Molecular Function	Transcription activator activity	9	CIITA, PPARA, FOXK1, ZMIZ2, MAML1, PAX8, TEAD1, FOXO1, NR5A2	0.43

riched pathways targeted by miRNA on Chr2.1 referring to its potential role in the modulation of activin signaling. miRNA on Chr19.1 potentially silences transcripts related to cell morphogenesis, similarly to miRNA on Chr1.1. In addition, it may inhibit the translation of a group of transcription activators. Due to the small number of targets predicted for miRNA on Chr15.1, no gene ontology terms became enriched.

Discussion

In the current study we presented, to our knowledge, for the first time the differential miRNA expression profiles of intrafollicular somatic cell populations, MGCs and CGCs, from human stimulated preovulatory follicles. Using NGS technology, we could detect annotated and novel miRNAs that provide new information on the basic biologic processes in the follicle via gene expression modulation.

Our data reveal that it is the miRNAs expressed at low levels that differentiated most significantly between CGCs and MGCs, and the most abundant miRNAs were highly similar between the cell types. In comparison with previous publications, there is a clear difference in the expression levels of abundant miRNAs, depending on whether follicular material or whole ovarian homogenates are analyzed (reviewed in Ref. 39). Therefore our results coincide best with those obtained from sheep follicular and luteal tissues (40): hsa-miR-21 being the most abundant miRNA, and hsa-miR-143-p, highly expressed in the ovarian homogenates of several mammals, is further behind in our top expression lists (22, 23, 41–43).

The mouse analog of hsa-miR-21 plays a role in granulosa cell survival during the transition from the follicular to luteal stage and is up-regulated by hCG-induced ovulation (44). Inhibition of this miRNA therefore leads to cell apoptosis (44). The second most abundant miRNA, hsa-let-7f, has been described as a tumor suppressor targeting aromatase mRNA in breast cancer cell lines (45). Aromatase, a key enzyme in estradiol biosynthesis, is evidently expressed in the ovarian follicle, proposing new potential roles for hsa-let-7f in the modulation of steroidogenesis. The third abundant miRNA in our data, hsa-miR-451a, is a proof of Dicer-independent miRNA biogenesis in granulosa cells. It has been the model miRNA for studying alternative pathways for miRNA generation, although by now it is clear that several other miRNAs are processed without Dicer (46). This finding may explain, in part, the relatively modest severity of the ovarian phenotype observed in conditional Dicer1 knock-out mice (19, 20).

The miRNA database miRBase is rapidly expanding with hundreds of new miRNA sequences added with every update. Therefore we were looking for unannotated miRNAs from our data, because human granulosa cells have not been studied in this regard. We identified 9 different novel miRNAs, 4 of which were expressed at a sufficient level for successful validation. Interestingly, 2 of the novel miRNAs (miRNA on Chr2.1 and miRNA on Chr15.1) are predictively transcribed from introns of 2 genes of high importance for folliculogenesis: FSHR and CYP19A1 (the gene encoding aromatase), respectively. It has been shown that by the end of follicle growth the expression of these 2 genes diminishes (47, 48). We currently have no knowledge, whether those miRNAs are coexpressed with their host genes or whether they are transcribed from independent promoters (49, 50). We also have no information on the role of the 2 miRNAs regarding the posttranscriptional regulation of their host genes. Both synergistic and antagonistic influences on the host gene mRNAs have been shown for intronic miRNAs (51, 52), and experimental validation is therefore necessary for each individual case. Our preliminary bioinformatic analysis did not confirm direct targeting of the host mRNAs by the 2 miRNAs. However, miRNA on Chr2.1 may be involved indirectly in the inhibition of FSHR expression. ACVR2B and SMAD2 are two members of the activin signaling cascade that are both predicted targets of miRNA on Chr2.1. Activin signaling leads to increase in FSHR mRNA expression in granulosa cells in the expansion stages of folliculogenesis (53, 54). If the elevated expression on FSHR mRNA leads to the coexpression of miRNA on Chr2.1 from FSHR intron, a negative feedback loop by targeting ACVR2B may be initiated, contributing to decreased FSHR expression by the preovulatory stage. Modulation of activin signaling by miRNAs has recently been studied in mouse, where mmu-miR-145 was experimentally confirmed to target ACVR2B mRNA in granulosa cells and inhibit their proliferation (55).

miRNA on Chr2.1 has high sequence similarity with the members of the hsa-miR-548 miRNA family. This is a group of miRNAs relatively new in evolution, only distinguishable in the primate lineage, that evolved together with a class of miniature inverted-repeat transposable elements Made1 (56). Our data therefore present further evidence that several new miRNAs will be discovered in known and unknown miRNA families when more cell and tissue types are investigated with sufficient depth.

In addition to providing new high-throughput data on miRNA expression, we were interested in determining the differentiating miRNA profiles and their roles between the human MGCs and CGCs. It is well known that a single miRNA may have several targets, and therefore

analyzing a group of miRNAs according to the ontology profiles of their targeted mRNAs is a common approach (57). However, there is no common tool for miRNA target prediction, and all available ones suffer from a high degree of both false-positive and false-negative results. Better prediction algorithms evolve together with experimental data on miRNA-mRNA binding sites. For higher confidence in estimating targets by bioinformatic methods, the use of mRNA data from the same system for comparison is suggested (57, 58). This approach is also not a golden standard, because not all posttranscriptional gene expression modifications can be evidenced on mRNA level, and several observed changes may be indirect (reviewed in Ref. 59). Therefore, although reducing the number of false predictions by using high-throughput mRNA and miRNA data together, the results should still be judged with caution. Another approach is to report overlapping data from several target prediction algorithms. This methodology may lead, on the other hand, to increased number of false-negative results with less true targets predicted.

Finding available miRNA target prediction software that is up to date with current miRBase is another challenge, as new miRNAs are constantly discovered and the database enlarges quickly. Therefore we used DIANA miRPath v.2.1 that is updated to miRBase v.18, the same version that was used for our small RNA NGS data analysis. Using this software, we only lost some miRNAs from analysis due to using very strict thresholds. As a second approach, we used IPA software that combines TargetScan, TarBase, and miRecords databases with our poly-A RNA seq results. With this method we lost data and obtained results for 25 miRNAs in CGCs and 19 miRNAs from MGCs (33 were uploaded in both cases).

TGFβ, ErbB, and heparan sulfate synthesis pathways were similarly targeted by miRNAs in MGCs and CGCs, although differentially expressed lists of miRNAs were used as input for bioinformatic analysis. The enrichment of these pathways is not surprising because their role in the fine-tuning of oocyte-somatic cell communication has appeared essential for follicular somatic cell differentiation and ovulation. The TGFβ family members Gdf9 and Bmp15 are the best studied mammalian oocyte-secreted factors that retain CGCs their specific molecular functions and inhibit their differentiation into MGCs (reviewed in Ref. 60). Recently, heparan sulfate proteoglycans (HSPGs) were shown to mediate the signaling of Gdf9 to CGCs in the mouse (61). The ErbB-signaling pathways modulate LH induction involved in COC expansion and follicular membrane rupture. More specifically, in mice the oocyte-secreted factors up-regulate the ErbB family member epidermal growth factor receptor expression in CGCs to enable these cells to respond to LH-induced signaling from MGCs (62). On the other hand, mouse CGCs were shown to express ErbB family ligands Areg and Nrg1, which promote oocyte developmental competence as well as progesterone production by MGCs (63). HSPG synthesis is up-regulated in MGCs of mammalian preovulatory follicles, and this is necessary for tissue remodeling during basal membrane rupture at ovulation (reviewed in Ref. 64). MGCs secrete HSPGs that bind antithrombin to maintain the fluidity of follicular fluid up to COC expulsion (65, 66). Interestingly, follicular fluid HSPGs contain 3-*O*-sulfated chains with unusually high frequency (66). According to our data, HS3ST1, the enzyme responsible for the side-chain addition, may be down-regulated by miRNAs in CGCs, proposing one more differential role for the granulosa cell types in the ovarian follicle. In MGCs we identified miRNAs targeting several ECM proteins: laminins, integrins, collagens, and fibronectin 1, providing further evidence of the fine tuning of tissue remodeling.

Members of the Wnt- and neurotrophin-signaling pathways were 2 differentially enriched groups of genes potentially targeted by miRNAs in MGCs. The down-regulated neurotrophin confirmed by the poly(A) RNA NGS in MGCs was brain-derived growth factor (BDNF), which corroborates with the results obtained from experimental data with human follicular cells. More precisely, CGCs, but not MGCs, secrete BDNF, the ligand for TrkB receptor that among follicular cells is expressed exclusively on oocytes (67–69). The signaling cascade upon TrkB activation is involved in the oocyte cytoplasmic maturation and the resumption of meiosis before ovulation (67–69). Although BDNF expression is significantly induced by LH and hCG in both granulosa cell populations in vitro, MGCs are incapable of secreting the protein (67, 69, 70).

The role of Wnt signaling in CGCs is not definitely clear in humans. This pathway is involved in cellular patterning, proliferation, survival, and modulation of LH stimulation in rodents and cows (71). However, conflicting results exist regarding the expression of some Wnt-signaling pathway proteins upon LH stimulation when rodent and human granulosa cells were compared (72–73). In addition, we have described several Wnt pathway genes expressed in human granulosa cells that have never been studied in relation to ovarian functions (demonstrated in the current study and in Ref. 13).

In conclusion, the current study provides new information on the posttranscriptional regulation of gene expression in the human stimulated preovulatory luteinizing

follicle. We have clearly shown the similarities and differences in miRNA expression between CGCs and MGCs and provided a bioinformatic prediction of their roles in various signaling pathways. Novel miRNAs from the introns of FSHR and aromatase genes provide new evidence of their mRNA processing, but their role during folliculogenesis remains to be determined. Importantly, the miRNA profile in granulosa cells may possess high potential as a new marker for successful folliculogenesis and oocyte developmental capacity.

Acknowledgments

We thank Janica Djupsjöbacka and Matti Kankainen from Biomedicum Functional Genomics Unit of Helsinki, Finland, for technical assistance. We are grateful to the staff of Nova Vita Clinic, Tallinn, Estonia, for recruiting the patients and collecting the samples, and to the women who participated in the study.

Address all correspondence and requests for reprints to: Agne Velthut-Meikas, Competence Centre on Reproductive Medicine and Biology, Tiigi 61B, 50410 Tartu, Estonia. E-mail: agnevelthut@gmail.com.

This work was supported by grant SF0180044s09 from the Estonian Ministry of Education and Research, by Grant EU30020 from Enterprise Estonia, and by the Academy of Finland and the Sigrid Jusélius Foundation.

Disclosure Summary: The authors have nothing to disclose.

References

1. **Diaz FJ, Wigglesworth K, Eppig JJ.** Oocytes determine cumulus cell lineage in mouse ovarian follicles. *J Cell Sci*. 2007;120(8):1330–1340.
2. **Oktem O, Oktay K.** The ovary: anatomy and function throughout human life. *Ann NY Acad Sci*. 2008;1127:1–9.
3. **Albertini DF, Combelles CM, Benecchi E, Carabatsos MJ.** Cellular basis for paracrine regulation of ovarian follicle development. *Reproduction*. 2001;121(5):647–653.
4. **Biggers JD, Whittingham DG, Donahue RP.** The pattern of energy metabolism in the mouse oöcyte and zygote. *Proc Natl Acad Sci USA*. 1967;58(2):560–567.
5. **Sánchez F, Smitz J.** Molecular control of oogenesis. *Biochim Biophys Acta*. 2012;1822(12):1896–1912.
6. **Hong SJ, Chiu PC, Lee KF, Tse JM, Ho PC, Yeung WS.** Establishment of a capillary-cumulus model to study the selection of sperm for fertilization by the cumulus oophorus. *Hum Reprod*. 2004;19(7):1562–1569.
7. **Jin M, Fujiwara E, Kakiuchi Y, et al.** Most fertilizing mouse spermatozoa begin their acrosome reaction before contact with the zona pellucida during in vitro fertilization. *Proc Natl Acad Sci USA*. 2011;108(12):4892–4896.
8. **Peng XR, Hsueh AJ, LaPolt PS, Bjersing L, Ny T.** Localization of luteinizing hormone receptor messenger ribonucleic acid expression in ovarian cell types during follicle development and ovulation. *Endocrinology*. 1991;129(6):3200–3207.
9. **Anderson RA, Sciorio R, Kinnell H, et al.** Cumulus gene expression as a predictor of human oocyte fertilisation, embryo development and competence to establish a pregnancy. *Reproduction*. 2009;138(4):629–637.
10. **Assidi M, Montag M, Van der Ven K, Sirard MA.** Biomarkers of human oocyte developmental competence expressed in cumulus cells before ICSI: a preliminary study. *J Assist Reprod Genet*. 2011;28(2):173–188.
11. **Grøndahl ML, Andersen CY, Bogstad J, Borgbo T, Hartvig Boujida VH, Borup R.** Specific genes are selectively expressed between cumulus and granulosa cells from individual human pre-ovulatory follicles. *Mol Hum Reprod*. 2012;18(12):572–584.
12. **Huang Z, Wells D.** The human oocyte and cumulus cells relationship: new insights from the cumulus cell transcriptome. *Mol Hum Reprod*. 2010;16(10):715–725.
13. **Kõks S, Velthut A, Sarapik A, et al.** The differential transcriptome and ontology profiles of floating and cumulus granulosa cells in stimulated human antral follicles. *Mol Hum Reprod*. 2010;16(4):229–240.
14. **Ouandaogo ZG, Frydman N, Hesters L, et al.** Differences in transcriptomic profiles of human cumulus cells isolated from oocytes at GV, MI and MII stages after in vivo and in vitro oocyte maturation. *Hum Reprod*. 2012;27(8):2438–2447.
15. **Chekulaeva M, Filipowicz W.** Mechanisms of miRNA-mediated post-transcriptional regulation in animal cells. *Curr Opin Cell Biol*. 2009;21(3):452–460.
16. **Krol J, Loedige I, Filipowicz W.** The widespread regulation of microRNA biogenesis, function and decay. *Nat Rev Genet*. 2010;11(9):597–610.
17. **Aalto AP, Pasquinelli AE.** Small non-coding RNAs mount a silent revolution in gene expression. *Curr Opin Cell Biol*. 2012;24(3):333–340.
18. **Szabó PM, Butz H, Igaz P, Rácz K, Hunyady L, Patócs A.** Minireview: MIRomics in endocrinology: a novel approach for modeling endocrine diseases. *Mol Endocrinol*. 2013;27(4):573–585.
19. **Lei L, Jin S, Gonzalez G, Behringer RR, Woodruff TK.** The regulatory role of Dicer in folliculogenesis in mice. *Mol Cell Endocrinol*. 2010;315(1–2):63–73.
20. **Nagaraja AK, Andreu-Vieyra C, Franco HL, et al.** Deletion of Dicer in somatic cells of the female reproductive tract causes sterility. *Mol Endocrinol*. 2008;22(10):2336–2352.
21. **Otsuka M, Zheng M, Hayashi M, et al.** Impaired microRNA processing causes corpus luteum insufficiency and infertility in mice. *J Clin Invest*. 2008;118(5):1944–1954.
22. **Landgraf P, Rusu M, Sheridan R, et al.** A mammalian microRNA expression atlas based on small RNA library sequencing. *Cell*. 2007;129(7):1401–1414.
23. **Huang J, Ju Z, Li Q, et al.** Solexa sequencing of novel and differentially expressed microRNAs in testicular and ovarian tissues in Holstein cattle. *Int J Biol Sci*. 2011;7(7):1016–1026.
24. **Ma T, Jiang H, Gao Y, et al.** Microarray analysis of differentially expressed microRNAs in non-regressed and regressed bovine corpus luteum tissue; microRNA-378 may suppress luteal cell apoptosis by targeting the interferon γ receptor 1 gene. *J Appl Genet*. 2011;52(4):481–486.
25. **Miles JR, McDaneld TG, Wiedmann RT, et al.** MicroRNA expression profile in bovine cumulus-oocyte complexes: possible role of let-7 and miR-106a in the development of bovine oocytes. *Anim Reprod Sci*. 2012;130(1–2):16–26.
26. **Lin F, Li R, Pan ZX, et al.** miR-26b promotes granulosa cell apoptosis by targeting ATM during follicular atresia in porcine ovary. *PLoS One*. 2012;7(6): e38640.
27. **Yao N, Yang BQ, Liu Y, et al.** Follicle-stimulating hormone regulation of microRNA expression on progesterone production in cultured rat granulosa cells. *Endocrine*. 2010;38(2):158–166.
28. **McCarthy DJ, Chen Y, Smyth GK.** Differential expression analysis of multifactor RNA-Seq experiments with respect to biological variation. *Nucleic Acids Res*. 2012;40(10):4288–4297.

29. **Robinson MD, McCarthy DJ, Smyth GK.** edgeR: a Bioconductor package for differential expression analysis of digital gene expression data. *Bioinformatics*. 2010;26(1):139–140.
30. **Friedländer MR, Mackowiak SD, Li N, Chen W, Rajewsky N.** miRDeep2 accurately identifies known and hundreds of novel microRNA genes in seven animal clades. *Nucleic Acids Res*. 2012; 40(1):37–52.
31. **Hofacker IL.** Vienna RNA secondary structure server. *Nucleic Acids Res*. 2003;31(13):3429–3431.
32. **Waterhouse AM, Procter JB, Martin DM, Clamp M, Barton GJ.** Jalview Version 2–a multiple sequence alignment editor and analysis workbench. *Bioinformatics*. 2009;25(9):1189–1191.
33. **Vlachos IS, Kostoulas N, Vergoulis T, et al.** DIANA miRPath v. 2.0: investigating the combinatorial effect of microRNAs in pathways. *Nucleic Acids Res*. 2012;40:W498–W504.
34. **Ogata H, Goto S, Sato K, Fujibuchi W, Bono H, Kanehisa M.** KEGG: Kyoto encyclopedia of genes and genomes. *Nucleic Acids Res*. 1999;27(1):29–34.
35. **Maragkakis M, Alexiou P, Papadopoulos GL, et al.** Accurate microRNA target prediction correlates with protein repression levels. *BMC Bioinformatics*. 2009;10:295.
36. **Maragkakis M, Reczko M, Simossis VA, et al.** DIANA-microT web server: elucidating microRNA functions through target prediction. *Nucleic Acids Res*. 2009;37(Web Server issue):W273–W276.
37. **Huang da W, Sherman BT, Lempicki RA.** Systematic and integrative analysis of large gene lists using DAVID bioinformatics resources. *Nat Protoc*. 2009;4(1):44–57.
38. **Huang da W, Sherman BT, Lempicki RA.** Bioinformatics enrichment tools: paths toward the comprehensive functional analysis of large gene lists. *Nucleic Acids Res*. 2009;37(1):1–13.
39. **Donadeu FX, Schauer SN, Sontakke SD.** Involvement of miRNAs in ovarian follicular and luteal development. *J Endocrinol*. 2012; 215(3):323–334.
40. **McBride D, Carré W, Sontakke SD, et al.** Identification of miRNAs associated with the follicular-luteal transition in the ruminant ovary. *Reproduction*. 2012;144(2):221–233.
41. **Hossain MM, Ghanem N, Hoelker M, et al.** Identification and characterization of miRNAs expressed in the bovine ovary. *BMC Genomics*. 2009;10:443.
42. **Li M, Liu Y, Wang T, et al.** Repertoire of porcine microRNAs in adult ovary and testis by deep sequencing. *Int J Biol Sci*. 2011;7(7): 1045–1055.
43. **Mishima T, Takizawa T, Luo SS, et al.** MicroRNA (miRNA) cloning analysis reveals sex differences in miRNA expression profiles between adult mouse testis and ovary. *Reproduction*. 2008;136(6): 811–822.
44. **Carletti MZ, Fiedler SD, Christenson LK.** MicroRNA 21 blocks apoptosis in mouse periovulatory granulosa cells. *Biol Reprod*. 2010;83(2):286–295.
45. **Shibahara Y, Miki Y, Onodera Y, et al.** Aromatase inhibitor treatment of breast cancer cells increases the expression of let-7f, a microRNA targeting CYP19A1. *J Pathol*. 2012;227(3):357–366.
46. **Langenberger D, Çakir MV, Hoffmann S, Stadler PF.** Dicer-Processed Small RNAs: Rules and Exceptions. *J Exp Zool B Mol Dev*. 2012;Evol:p. 1–12.
47. **Hernandez-Gonzalez I, Gonzalez-Robayna I, Shimada M, et al.** Gene expression profiles of cumulus cell oocyte complexes during ovulation reveal cumulus cells express neuronal and immune-related genes: does this expand their role in the ovulation process? *Mol Endocrinol*. 2006;20(6):1300–1321.
48. **Jeppesen JV, Kristensen SG, Nielsen ME, et al.** LH-receptor gene expression in human granulosa and cumulus cells from antral and preovulatory follicles. *J Clin Endocrinol Metab*. 2012;97(8): E1524–E531.
49. **Baskerville S, Bartel DP.** Microarray profiling of microRNAs reveals frequent coexpression with neighboring miRNAs and host genes. *RNA*. 2005;11(3):241–247.
50. **Monteys AM, Spengler RM, Wan J, et al.** Structure and activity of putative intronic miRNA promoters. *RNA*. 2010;16(3):495–505.
51. **Hinske LC, Galante PA, Kuo WP, Ohno-Machado L.** A potential role for intragenic miRNAs on their hosts' interactome. *BMC Genomics*. 2010;11:533.
52. **Lutter D, Marr C, Krumsiek J, Lang EW, Theis FJ.** Intronic microRNAs support their host genes by mediating synergistic and antagonistic regulatory effects. *BMC Genomics*. 2010;11:224.
53. **Minegishi T, Kishi H, Tano M, Kameda T, Hirakawa T, Miyamoto K.** Control of FSH receptor mRNA expression in rat granulosa cells by 3′,5′-cyclic adenosine monophosphate, activin, and follistatin. *Mol Cell Endocrinol*. 1999;149(1–2):71–77.
54. **Myers M, van den Driesche S, McNeilly AS, Duncan WC.** Activin A reduces luteinisation of human luteinised granulosa cells and has opposing effects to human chorionic gonadotropin in vitro. *J Endocrinol*. 2008;199(2):201–212.
55. **Yan G, Zhang L, Fang T, et al.** MicroRNA-145 suppresses mouse granulosa cell proliferation by targeting activin receptor IB. *FEBS Lett*. 2012;586(19):3263–3270.
56. **Piriyapongsa J, Jordan IK.** A family of human microRNA genes from miniature inverted-repeat transposable elements. *PLoS One*. 2007;2(2):e203.
57. **Ritchie W, Flamant S, Rasko JE.** Predicting microRNA targets and functions: traps for the unwary. *Nat Methods*. 2009;6(6):397–398.
58. **Lim LP, Lau NC, Garrett-Engele P, et al.** Microarray analysis shows that some microRNAs downregulate large numbers of target mRNAs. *Nature*. 2005;433(7027):769–773.
59. **Pasquinelli AE.** MicroRNAs and their targets: recognition, regulation and an emerging reciprocal relationship. *Nat Rev Genet*. 2012; 13(4):271–282.
60. **Paulini F, Melo EO.** The role of oocyte-secreted factors GDF9 and BMP15 in follicular development and oogenesis. *Reprod Domest Anim*. 2011;46(2):354–361.
61. **Watson LN, Mottershead DG, Dunning KR, Robker RL, Gilchrist RB, Russell DL.** Heparan sulfate proteoglycans regulate responses to oocyte paracrine signals in ovarian follicle morphogenesis. *Endocrinology*. 2012;153(9):4544–4555.
62. **Park JY, Su YQ, Ariga M, Law E, Jin SL, Conti M.** EGF-like growth factors as mediators of LH action in the ovulatory follicle. *Science*. 2004;303(5658):682–684.
63. **Noma N, Kawashima I, Fan HY, et al.** LH-induced neuregulin 1 (NRG1) type III transcripts control granulosa cell differentiation and oocyte maturation. *Mol Endocrinol*. 2011;25(1):104–116.
64. **de Agostini A.** An unexpected role for anticoagulant heparan sulfate proteoglycans in reproduction. *Swiss Med Wkly*. 2006;(136): 583–590.
65. **Princivalle M, Hasan S, Hosseini G, de Agostini AI.** Anticoagulant heparan sulfate proteoglycans expression in the rat ovary peaks in preovulatory granulosa cells. *Glycobiology*. 2001;11(3):183–194.
66. **de Agostini AI, Dong JC, de Vantéry Arrighi C, et al.** Human follicular fluid heparan sulfate contains abundant 3-O-sulfated chains with anticoagulant activity. *J Biol Chem*. 2008;283(42):28115–28124.
67. **Seifer DB, Feng B, Shelden RM, Chen S, Dreyfus CF.** Brain-derived neurotrophic factor: a novel human ovarian follicular protein. *J Clin Endocrinol Metab*. 2002;87(2):655–659.
68. **Kawamura K, Kawamura N, Mulders SM, Sollewijn Gelpke MD, Hsueh AJ.** Ovarian brain-derived neurotrophic factor (BDNF) promotes the development of oocytes into preimplantation embryos. *Proc Natl Acad Sci USA*. 2005;102(26):9206–9211.
69. **Zhao P, Qiao J, Huang S, et al.** Gonadotrophin-induced paracrine regulation of human oocyte maturation by BDNF and GDNF secreted by granulosa cells. *Hum Reprod*. 2011;26(3):695–702.
70. **Dominguez MA, Cho N, Zhang B, Neal MS, Foster WG.** Brain-

derived neurotrophic factor expression in granulosa lutein cells. *Reprod Biomed Online*. 2011;22(1):17–24.
71. **Boyer A, Goff AK, Boerboom D.** WNT signaling in ovarian follicle biology and tumorigenesis. *Trends Endocrinol Metab*. 2010;21(1):25–32.
72. **Hsieh M, Mulders SM, Friis RR, Dharmarajan A, Richards JS.** Expression and localization of secreted frizzled-related protein-4 in the rodent ovary: evidence for selective up-regulation in luteinized granulosa cells. *Endocrinology*. 2003;144(10):4597–45606.
73. **Maman E, Yung Y, Cohen B, et al.** Expression and regulation of sFRP family members in human granulosa cells. *Mol Hum Reprod*. 2011;17(7):399–404.